Ab initio calculations of temperature-dependent magnetostriction of Fe and $A2$ Fe$_{1-x}$Ga$_x$ within the disordered local moment picture

George A. Marchant, Christopher E. Patrick, and Julie B. Staunton[*]

Department of Physics, University of Warwick, Coventry CV4 7AL, United Kingdom

The fully relativistic disordered local moment (DLM) theory is used to perform calculations of the magnetic torque of tetragonally distorted Fe and fully disordered ($A2$) Fe$_{1-x}$Ga$_x$ ($0 \leqslant x \leqslant 0.2$) alloys to describe the temperature dependence of their magnetoelasticity. The finite-temperature magnetoelasticity, in particular the magnetoelastic constant B_1, is obtained within DLM theory by studying the response of the magnetic torque generated by the magnetocrystalline anisotropy to the application of a tetragonal strain. Calculations of B_1 have been performed on bcc Fe across its ferromagnetic temperature range. Our results show good qualitative agreement with experiment, in particular reproducing the anomalous, nonmonotonic thermal behavior of bcc Fe's magnetostriction, which has been largely unexplained for more than 50 years. The method has also been used to calculate the finite-temperature magnetoelasticity of the $A2$ phase of Fe$_{1-x}$Ga$_x$ alloys as a starting point for further investigations into the giant magnetostriction of Galfenol alloys. Our calculations show that homogeneously doping bcc Fe with Ga does not produce an enhancement in magnetostriction and that the nonmonotonic temperature dependence and significant volume dependence are suppressed by increasing Ga content.

I. INTRODUCTION

Magnetostriction, the deformation experienced by materials due to the application of a magnetic field, is a phenomenon potentially useful in sensor and actuator technologies, providing a method of converting between mechanical and electrical energy [1]. The discovery of the giant magnetostrictive properties of Tb$_{1-x}$Dy$_x$Fe$_2$ (Terfenol-D) in the 1970s [2] continues to inspire research efforts devoted to both building magnetostrictive devices [3] and searching for new magnetostrictive materials [4]. A relatively recently discovered class of magnetostrictive materials are the Fe-based alloys Fe-Ga and Fe-Al (Galfenol and Alfenol) [5,6] which, although having inferior magnetostrictive properties to Terfenol-D, are attractive due to their low cost and high mechanical strength [7]. Fundamentally, it is intriguing that by adding only a small amount (∼19%) of the nonmagnetic elements Al and Ga, an alloy is formed whose magnetostrictive properties are greatly enhanced (∼10× for Galfenol) compared to elemental Fe [5].

For practical applications it is essential to understand how a material's magnetostrictive properties vary as a function of temperature. In systems where the magnetic moments originate from highly localized electrons, such as the rare earths [8], the single-ion model established in the seminal works of Callen and Callen [9,10] provides an excellent description of finite-temperature magnetostrictive behavior [11]. However, the magnetism in Fe and its alloys originates from itinerant electrons, so that it is by no means obvious that the single-ion model should apply [12]. Indeed, it was recognized by Callen and Callen in 1963 that the single-ion model was at variance

with experimental measurements of the magnetostriction of pure and Si-doped Fe, which showed a nonmonotonic temperature dependence [13,14]. Although proposing an explanation in that work based on anisotropic magnon-phonon coupling [14], subsequent experiments [15–17] led E. Callen to write thirty years later that the temperature dependence of the magnetostriction of Fe was still not understood [1], and to the current authors' knowledge this situation remains. An interesting hint regarding the magnetostriction of Fe has however been provided by empirical calculations based on a tight-binding model, which showed that a nonmonotonic temperature dependence could arise as a result of a temperature-dependent electronic band structure [18]. In order to accurately model these temperature-dependent magnetic properties, it is key to describe the effect of fluctuations of magnetic degrees of freedom. The disordered local moment (DLM) picture [19] has proven to be an effective approach [20–24] to this problem. It utilizes the fact that, for many materials, thermally induced reorientations of local magnetic moments take place on a far slower timescale than the motion of the electrons. With a suitable method for determining ensemble averages over these orientational configurations, the temperature dependence of various magnetic properties can be determined nonempirically (*ab initio*). Until now it has not been used to study a system's magnetostriction however.

In terms of nonempirical band structure calculations at *zero temperature*, the last twenty years have seen significant progress in the calculation of magnetostriction within density functional theory (DFT) [25]. Due to the spin-orbit origin of magnetostriction, such calculations must be performed relativistically and be able to resolve energy differences of order 0.01 meV/atom [26]. Despite these technical challenges, the magnetostriction along the [0 0 1] axis calculated within DFT

*j.b.staunton@warwick.ac.uk

for the bulk ferromagnets Fe, Ni, and Co agrees qualitatively (i.e., having opposite signs for Fe/Co and Ni) and quantitatively (for Co and Ni) with experimental measurements [27–31]. Fe remains slightly problematic, with the calculations predicting the opposite sign to experiment for distortion along the [1 1 1] direction [32] and overestimating the [0 0 1] magnetostriction by a factor of 2–3 [30]. However given the smallness of the numbers involved (a fractional distortion of 22 parts per million along the [0 0 1] direction) [17] the level of agreement in the latter is arguably still good.

In addition to studies of the zero-temperature magnetostriction of elemental Fe, *ab initio* calculations have also been employed to investigate the properties of Fe-Ga alloys [33–38], particularly with regard to the enhanced magnetostriction at ~19% Ga content [5]. Early calculations employed relatively small simulation cells to calculate the properties of ordered phases at particular stoichiometries, e.g., Fe_3Ga, where it was found that the magnetostriction was highly sensitive to the type of ordering [33]. Larger supercells allowed the investigation of different stoichiometries, where an increase in magnetostriction was observed with Ga content [34]. Most recently, by using *ab initio* molecular dynamics simulations of 128-atom supercells to simulate disordered $Fe_{1-x}Ga_x$ structures, a peak in magnetostriction was calculated to occur at $x = 0.19$ [35]. The drop in magnetostriction at larger x was assigned to the development of $D0_3$-type ordering, which (for Fe_3Ga) was previously calculated to have negative magnetostriction [33]. Interestingly, Ref. [35] did not find a particular correlation between increased magnetostriction and $B2$-type ordering, which had previously been proposed [33].

Rather than using supercells, an alternative method of simulating compositional disorder is to use the coherent-potential approximation (CPA) [39]. Reference [38] used this approach to calculate the energetics, electronic structure, and magnetizations of different $Fe_{1-x}Ga_x$ phases ($A2$, $B2$, and $D0_3$). The advantage of the CPA is its ability to handle arbitrary compositions [38]. However, the authors of Ref. [38] conclude that, if the increase in magnetostriction with Ga content is a consequence of the local Fe environment being modified, i.e., short-range ordering or clustering, the CPA calculations (which treat disorder through a single-site effective medium approach neglecting short-range order) will not capture such an effect.

It is important to note that an alternative explanation exists for the magnetostriction behavior of $Fe_{1-x}Ga_x$ in terms of extrinsic effects. References [40,41] establish a model where tetragonal nanoheterogeneities rotate under the application of a magnetic field and enhance the magnetostriction. Although a number of experimental studies have reported the presence of such tetragonal nanoheterogeneities [42–44], others have argued that they do not play a key role [45,46]. Given this uncertainty it is essential to fully characterize the intrinsic contribution to the magnetostriction.

In this paper we present *ab initio* calculations of the intrinsic magnetostriction of elemental Fe and $A2$ $Fe_{1-x}Ga_x$. Unlike previous DFT-based calculations of magnetostriction in the literature [26–30,33–35], finite-temperature effects are included within the DLM picture [19] in which the averaging over orientational configurations of the local moments is also handled using the CPA. We focus on the tetragonal [0 0 1]

distortion, which for elemental Fe has an anomalous temperature dependence [17]. While our method could in principle be applied also to study a [1 1 1] distortion, we do not address it in this current study owing to the greater difficulty in obtaining an accurate description of this by $T = 0$ K DFT calculations [32].

Our calculations show a high sensitivity of the magnetostriction to the Fe lattice parameter and a strongly nonmonotonic temperature dependence. For $Fe_{1-x}Ga_x$ we consider the fully disordered $A2$ phase, treating Ga doping within the CPA. Such calculations do not reveal any large enhancement in the magnetostriction with increased Ga doping. Furthermore the increase in Ga content suppresses the nonmonotonic temperature dependence observed in elemental Fe.

The rest of our paper is ordered as follows. In Sec. II we describe our method of calculating the finite-temperature magnetostriction. In Sec. III we present the results of our calculations on elemental Fe (Sec. III A) and $A2$ $Fe_{1-x}Ga_x$ for $0 \leqslant x \leqslant 0.2$ (Sec. III B). Finally in Sec. IV we summarize our results.

II. THEORY

A. Magnetoelastic coupling

A cubic, magnetized material placed under a strain quantified by the tensor ε_{ij} will acquire two additional contributions to its total energy [47]. The first contribution is a magnetization-independent elastic energy E_{el} characterized by the elastic constants c_{ij}:

$$E_{el} = \tfrac{1}{2}c_{11}\left(\varepsilon_{xx}^2 + \varepsilon_{yy}^2 + \varepsilon_{zz}^2\right) + \tfrac{1}{2}c_{44}\left(\varepsilon_{xy}^2 + \varepsilon_{yz}^2 + \varepsilon_{zx}^2\right)$$
$$+ c_{12}(\varepsilon_{xx}\varepsilon_{yy} + \varepsilon_{yy}\varepsilon_{zz} + \varepsilon_{zz}\varepsilon_{xx}). \quad (1)$$

The second contribution is the magnetoelastic energy, which depends both on the strain and also on the magnetization direction $\hat{\boldsymbol{n}}$, which is written in terms of the direction cosines α_i [$\hat{\boldsymbol{n}} = (\alpha_x, \alpha_y, \alpha_z)$]. The contribution linear in strain is characterized by the magnetoelastic constants B_1 and B_2:

$$E_{me} = B_1\left(\alpha_x^2\varepsilon_{xx} + \alpha_y^2\varepsilon_{yy} + \alpha_z^2\varepsilon_{zz}\right)$$
$$+ B_2(\alpha_x\alpha_y\varepsilon_{xy} + \alpha_y\alpha_z\varepsilon_{yz} + \alpha_z\alpha_x\varepsilon_{zx}). \quad (2)$$

In principle E_{me} also contains a contribution independent of magnetization direction with magnetoelastic constant B_0, which vanishes for volume-conserving deformations ($\varepsilon_{xx} + \varepsilon_{yy} + \varepsilon_{zz} = 0$) [48].

The form of the magnetoelastic energy E_{me} arises from basic symmetry considerations, irrespective of the underlying physical mechanism [47]. In the systems studied here it is the spin-orbit interaction which couples the total energy of the system to the magnetization direction $\hat{\boldsymbol{n}}$, generating the magnetocrystalline anisotropy (MCA). Now specializing to the case of a volume-conserving tetragonal deformation for a system magnetized along the [0 0 1] direction ($\varepsilon_{xx} = \varepsilon_{yy} = -\varepsilon_{zz}/2$; $\varepsilon_{ij} = 0$ for $i \neq j$; $\alpha_z = 1$; $\alpha_x = \alpha_y = 0$), the contribution to the energy is

$$E([001]) = \tfrac{3}{4}\varepsilon_{zz}^2(c_{11} - c_{12}) + B_1\varepsilon_{zz}. \quad (3)$$

Minimizing $E([001])$ with respect to the strain ε_{zz}, and labeling the equilibrium value of ε_{zz} as λ_{001} (the fractional length

change in the [0 0 1] direction), gives the standard result [48]:

$$\lambda_{001} = -\frac{2}{3}\frac{B_1}{c_{11} - c_{12}}. \qquad (4)$$

The magnetostriction constant λ_{001} can be determined experimentally through the use of the strain gauge technique [49], which along with experimental determinations of the elastic moduli and Eq. (4) can be used to deduce the magnetoelastic constant B_1.

B. Magnetic torque and magnetoelasticity

To calculate B_1, we consider a system strained along the [0 0 1] direction ($\varepsilon_{zz} = u$) with all other strain components set to zero. The angular-dependent magnetoelastic contribution to the energy is then simply

$$E(u, \alpha_z) = B_1 u \alpha_z^2. \qquad (5)$$

Rotating the magnetization away from its preferred direction yields a torque, whose azimuthal component $T_\theta = -\partial E/\partial\theta$ where $\cos\theta = \alpha_z$, $\sin\theta\cos\phi = \alpha_x$, and $\sin\theta\sin\phi = \alpha_y$. Fixing $\theta = 45°$ gives

$$T_{\theta=45°} = B_1 u. \qquad (6)$$

The magnetoelastic constants can thus be understood as the linear response of the magnetic torque to the structural distortion. A distinction should be drawn between the artificial strain that is used here to determine B_1 and the real strain that is observed in experiment. The latter is governed by the system's Poisson ratio ν, meaning that a strain in the z axis is coupled with perpendicular strains such that $\nu = -\varepsilon_{xx}/\varepsilon_{zz} = -\varepsilon_{yy}/\varepsilon_{zz}$. It is not required that the simulated strain maintain Poisson's ratio however, as its purpose is only to determine B_1.

The torque method introduced in Ref. [50] allows T_θ to be calculated within a zero-temperature DFT framework. The method was extended to finite temperature in Refs. [20] and [21] within the DFT-DLM picture and has since been used to calculate the MCA of various materials [22,23]. By calculating the torque as a function of strain at different temperatures, we can obtain the temperature dependence of the magnetoelastic constant B_1. For convenience we summarize the key concepts of the DFT-DLM picture in the following section. A more thorough description can be found in Refs. [19,21,51].

The form of the dependence of the magnetoelastic torque on magnetization direction calculated by our method is investigated in the Supplemental Material [52], where it is confirmed that the form derived from Eq. (5) is sufficient.

C. The disordered local moment picture

1. Overview

DLM theory can be applied if one is able to establish that a system's magnetic temperature dependence is controlled primarily by the thermally induced disorder of "good" local moments emerging from the systems' interacting electrons, which maintain their magnitudes as temperature is increased. (This approach can be extended to systems where local moments emerge cooperatively on clusters of sites [53].) The system is treated as a lattice with each unit cell having its own magnetic orientation and with the orientations distributed according to appropriately determined statistical mechanics.

This picture is rigorous in many materials as the timescale τ on which electrons arrive at and leave a site is much faster than the fluctuation of the spin orientation on that site. It is thus possible for that site i to have a nonzero magnetization when it is time-averaged over τ, the direction of which is $\hat{\boldsymbol{e}}_i = (\sin\theta_i'\cos\phi_i', \sin\theta_i'\sin\phi_i', \cos\theta_i')$. The average direction of magnetization is denoted $\hat{\boldsymbol{n}}$.

The thermodynamic grand potential Ω is the system Hamiltonian that could in principle be determined within constrained DFT on an appropriately large unit cell, which provides the probability distribution

$$P(\{\hat{\boldsymbol{e}}_i\}) = \frac{1}{Z}\exp\left[-\beta\Omega(\{\hat{\boldsymbol{e}}_i\})\right], \qquad (7)$$

where Z is the corresponding partition function [19]. Due to the inherent complexity of the electronic grand potential, it is necessary to devise a trial Hamiltonian $\bar{\Omega}_0(\{\hat{\boldsymbol{e}}\})$. We utilize the mean-field approximation

$$\bar{\Omega}_0(\{\hat{\boldsymbol{e}}\}) = -\sum_i \boldsymbol{h}_i \cdot \hat{\boldsymbol{e}}_i, \qquad (8)$$

where $\boldsymbol{h}_i$ are denoted the Weiss fields. The Weiss fields are chosen to minimize the quantity $\mathcal{F} = F_0 + \langle\Omega\rangle_T - \langle\bar{\Omega}_0\rangle_T$ which is an upper bound to the exact free energy [19], where F_0 is the free energy associated with $\bar{\Omega}_0$ and the thermal averages $\langle\rangle_T$ at a temperature T are performed with respect to the trial Hamiltonian. As emphasized in studies which have looked at magnetic phase diagrams [54,55] and magnetic anisotropy [21] using DLM theory, at no stage is there any assumption of pairwise-only interactions among the local moments. All higher-order terms such as bilinear quartic terms are included within this description. Performing the minimization yields the expression for the Weiss fields,

$$\boldsymbol{h}_i = \frac{3}{4\pi}\int \hat{\boldsymbol{e}}_i \langle\Omega\rangle_{\hat{\boldsymbol{e}}_i} d\hat{\boldsymbol{e}}_i. \qquad (9)$$

The notation $\langle X \rangle_{\hat{\boldsymbol{e}}_i}$ represents a partial average, which in this context means to take an ensemble average that excludes the specified orientation $\hat{\boldsymbol{e}}_i$. With the trial Hamiltonian probability distribution reducing to a product over single-site probabilities,

$$P^0(\{\hat{\boldsymbol{e}}_i\}) = \frac{1}{Z_0}\exp\left[-\beta\bar{\Omega}_0(\{\hat{\boldsymbol{e}}_i\})\right] = \prod_i P_i^0(\hat{\boldsymbol{e}}_i), \qquad (10)$$

one can determine analytical expressions of ensemble averages, the most important of which being the magnetic order parameter

$$\boldsymbol{m}_i = \int \hat{\boldsymbol{e}}_i P_i^0(\hat{\boldsymbol{e}}_i) d\hat{\boldsymbol{e}}_i = \hat{\boldsymbol{h}}_i L(\beta h_i), \qquad (11)$$

where $L(x) = 1/\tanh(x) - 1/x$, which is proportional to the magnetization and aligns with the local Weiss field ($\beta = 1/k_B T$). In ferromagnetic systems $m(T)$ is equivalent to the reduced magnetization $M(T)/M(0)$, and we shall refer to this quantity extensively in what follows.

2. Calculation of magnetic torques

The temperature-dependent magnetic torque is calculated in DLM theory as the angular derivative of $\mathcal{F}$, i.e., $T_\theta = -\partial \mathcal{F}/\partial \theta$ [21]. By writing $\mathcal{F}$ as

$$\mathcal{F} = \langle \Omega \rangle_T + \frac{1}{\beta} \sum_i \int P_i^0(\hat{\mathbf{e}}_i) \ln P_i^0(\hat{\mathbf{e}}_i) d\hat{\mathbf{e}}_i, \qquad (12)$$

and noting that only the grand-potential term varies with respect to the direction of magnetization, we have

$$T_\theta = -\frac{\partial}{\partial \theta} \left[\sum_i \int P_i^0(\hat{\mathbf{e}}_i) \langle \Omega \rangle_{\hat{e}_i} d\hat{\mathbf{e}}_i \right]. \qquad (13)$$

A more complete description of the torque method in the context of DLM theory is provided in Ref. [21].

3. Coherent-potential approximation

The essential ingredient required to calculate the torque and Weiss fields is the partial average of the grand potential $\langle \Omega \rangle_{\hat{e}_i}$ [Eqs. (9) and (10)], which can be calculated using the coherent-potential approximation (CPA) alongside Korringa-Kohn-Rostocker (KKR) multiple-scattering theory [39,56]. Here the CPA is used for both treating the chemical disorder in $Fe_{1-x}Ga_x$ and the magnetic disorder at finite temperature. The requirement upon which the system is solved is that an average of all substituted $\hat{e}$'s reproduces the scattering of the disordered system as a whole. KKR multiple-scattering theory naturally builds these disordered (rotated) single-site scattering t matrices via unitary rotation operators.

D. Computational details

The steps taken to calculate the magnetoelastic constant B_1 at finite temperature within the DFT-DLM picture are as follows:

(1) Perform a self-consistent, scalar-relativistic calculation on the unstrained (cubic) system with all magnetic moments ferromagnetically aligned, including compositional disorder (for $Fe_{1-x}Ga_x$) at the level of the CPA.

(2) Using the "frozen" atom-centered potentials generated in the first step, perform a non-self-consistent, fully relativistic calculation on a strained structure where the magnetic disorder is characterized by the order parameter m [Eq. (11)] magnetized along the direction $\hat{\mathbf{n}} = (1, 0, 1)/\sqrt{2}$. We choose strains in the range $-0.01 \leqslant u \leqslant 0.01$.

(3) Repeat the second step for a set of strains in order to calculate the torque $T_{\theta=45°}$ as a function of u, and extract B_1 as the linear coefficient [Eq. (6)].

(4) Repeat steps 2 and 3 for different degrees of magnetic disorder m.

The scalar-relativistic calculations in step 1 are performed using the KKR-CPA HUTSEPOT code [57]. We treat the DFT exchange correlation at the level of the local spin-density approximation (LSDA) [58] and use the muffin tin approximation for the potential. The Brillouin zone was sampled on a $30 \times 30 \times 30$ grid and the angular momentum expansions were truncated at $l_{max} = 3$. In step 2 we use our own code to solve the Kohn-Sham-Dirac and CPA equations to obtain the Weiss fields and torques [21]. We use an adaptive Brillouin
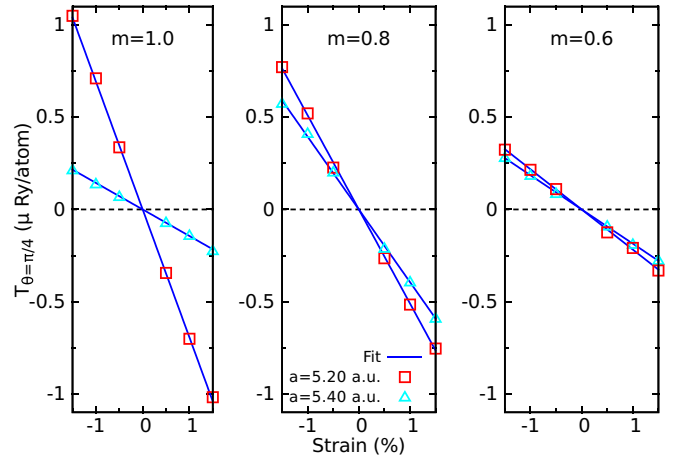

FIG. 1. Torques T_θ calculated for bcc Fe magnetized along the direction $\hat{\mathbf{n}} = (1, 0, 1)/\sqrt{2}$ with a strain applied along the [0 0 1] direction, for different magnetic order parameters m.

zone sampling scheme [59], with the magnetic moment orientations sampled in a 250×40 grid that is equally spaced in $\cos \theta'$ and ϕ', in order to obtain the necessary numerical precision to resolve the magnetoelastic coupling energies, and perform the energy integrals in the complex plane [60]. Due to the spin-orbit interaction and also the magnetic disorder, it is necessary to carefully adjust the Fermi energy between the scalar ferromagnetic and fully relativistic DLM calculations, so that integrating the calculated density of states yields the correct number of electrons per unit cell [22]. The effects of different approximations, such as the atomic sphere or muffin tin approximations, the use of potentials from a paramagnetic DLM state or from the $T = 0$ K ferromagnetic state, and whether the potentials in step 1 are generated in the strained system rather than the cubic one are described in the Supplemental Material [52].

III. RESULTS AND DISCUSSION

A. bcc Fe

1. Extracting B_1

We begin by illustrating our method of extracting B_1 from the torque calculations. Figure 1 shows $T_{\theta=45°}$ calculated as a function of strain for three values of the magnetic order parameter m, namely $m = 1.0$, 0.8, and 0.6; $m = 1.0$ corresponds to the fully ordered, zero-temperature state. We show data calculated with the cubic lattice parameter a set to 5.20 or 5.40 bohr radii (atomic units, a.u.). 5.20 a.u. (squares in Fig. 1) corresponds to the zero-temperature bcc Fe lattice constant obtained from the scalar-relativistic KKR calculations within the LSDA and muffin tin approximation, while 5.40 a.u. (triangles) corresponds to the low-temperature lattice constant measured experimentally [61].

The straight line fits of the data of Fig. 1 confirm the linear relation between torque and strain described by Eq. (6). The negative gradient implies a negative value of B_1, and therefore a positive magnetostriction through Eq. (4). However, clearly both the zero-temperature ($m = 1$) value of B_1 and its evolution with temperature depend strongly on which cubic lattice
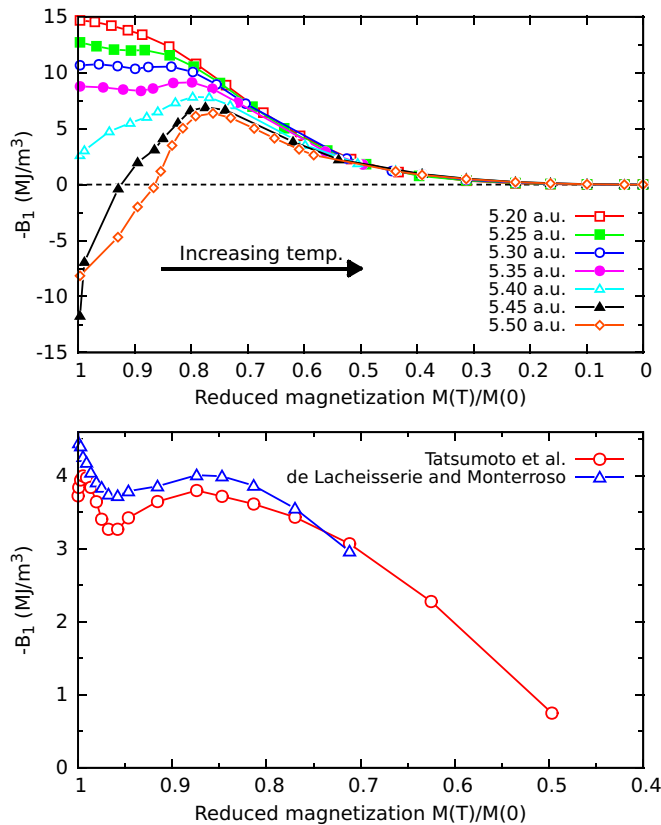
FIG. 2. Top: The variation in the (negative) magnetoelastic constant B_1 with respect to reduced magnetization m for lattice parameters between 5.20 a.u. and 5.50 a.u. in bcc Fe. Bottom: The experimentally measured magnetoelastic constant B_1 of bcc Fe, extracted from magnetostriction [13,17] and elastic constant [62,63] data and plotted in terms of the reduced magnetization $m = M(T)/M(0)$ (cf. Appendix A). Blue triangles correspond to magnetostriction data from Ref. [17] and red circles from Ref. [13].

constant is used. Using the theoretical lattice constant of 5.20 a.u. finds B_1 to decrease in magnitude as the moments become more disordered, while at the experimental lattice constant of 5.40 a.u. the magnitude of B_1 undergoes a peak (steeper gradient) at $m = 0.8$ compared to $m = 1$ and 0.6.

2. Volume dependence of B_1

To further investigate the dependence of B_1 on the bcc lattice constant, we extend the calculations shown in Fig. 1 to cover the full range of magnetizations $0 \leqslant m \leqslant 1$ and lattice parameters 5.20–5.50 a.u. This range includes the lattice parameter measured at the Curie temperature 1040 K of 5.47 a.u. [61]. The data are plotted in Fig. 2.

Considering the zero-temperature ($m = 1$) data first, we calculate a monotonic shift in B_1 to more positive values as the lattice parameter is increased from 5.20 to 5.45 a.u. Expanding the lattice further to 5.50 a.u. results in a reduction in B_1. The dependence of B_1 on volume is very strong, particularly around the experimental lattice parameter of 5.40 a.u. Between $a = 5.40$ and 5.45 a.u. B_1 changes sign, i.e., going from positive to negative magnetostriction.

As the temperature increases (decreasing m) the behavior of B_1 is also dependent on volume. At the theoretical lattice constant the magnitude of B_1 decreases monotonically. As the lattice parameter is increased beyond 5.35 a.u. a second feature develops, which is a peak in the magnitude of B_1 at values of m between 0.7–0.8. This peak remains even at larger lattice spacings when the zero-temperature magnetostriction has changed sign. At higher temperatures ($m < 0.6$) the data for the various lattice parameters effectively coalesce, vanishing at the Curie point $m = 0$.

3. Comparison to experiment and previous calculations

As discussed in Sec. II A, experiments do not provide direct access to B_1 but rather measure the fractional change in length λ_{001}. In Appendix A we describe the conversion of reported λ_{001} [13,17] and elastic constant [62,63] values into B_1, and also the conversion of temperature into reduced magnetization [64,65]. The bottom half of Fig. 2 shows the resulting values of B_1, derived from two different sets of magnetostriction measurements reported in Refs. [13] and [17]. The experimentally measured values of B_1 show an initial decrease in magnitude with temperature, followed by an increase to a maximum value at $m = 0.85$ before decreasing again. As described in the Introduction, the origin of this nonmonotonic behavior has been debated for well over 50 years [1,14,18]. Although there is disagreement among experimental studies about the presence of another peak in B_1 at much lower temperature [13,16,17], the peak at $m = 0.85$ is consistently observed, and results in an enhancement in the magnetostriction λ_{001} of $\sim 50\%$ at 800 K compared to its zero-temperature value [17].

Now considering our calculations, concentrating on zero temperature first, we note that calculations at both the theoretical and experimental lattice parameters (5.20 and 5.40 a.u.) yield a negative B_1 as in experiment. Indeed the calculated values of B_1 are reasonably close to experiment, ranging between -15.0 and -2.5 MJ m^{-3} compared to the experimental values of -3.3 [13] and -4.4 MJ m^{-3} [17]. Previous zero-temperature calculations based on the LSDA but using different methodologies (e.g., full potential rather than the muffin tin approximation) also found values for B_1 in the range between -7.4 and -10.1 MJ m^{-3} when using theoretical lattice parameters [28,29], while Ref. [30] found that at the experimental lattice parameter $B_1 = -8.3$ MJ m^{-3}. Our study investigates the effect on B_1 of systematically varying the lattice constant.

Going beyond zero temperature, we compare the temperature dependence of B_1 calculated *ab initio* to experiment (Fig. 2). It is very encouraging to observe that the anomalous peak in the magnitude of B_1 observed experimentally appears also in the calculations, for a wide range of lattice constants ($\pm 2\%$ of the experimental value of 5.40 a.u.). Given that the calculations are performed with static ions and no impurities, our results support the idea that the nonmonotonic behavior of B_1 in bcc Fe is an intrinsic effect distinct from magnon-phonon coupling [14], and instead can be explained in terms of the finite-temperature magnetic disorder inducing changes in the electronic structure [18] and enhancing the magnetoelastic coupling.
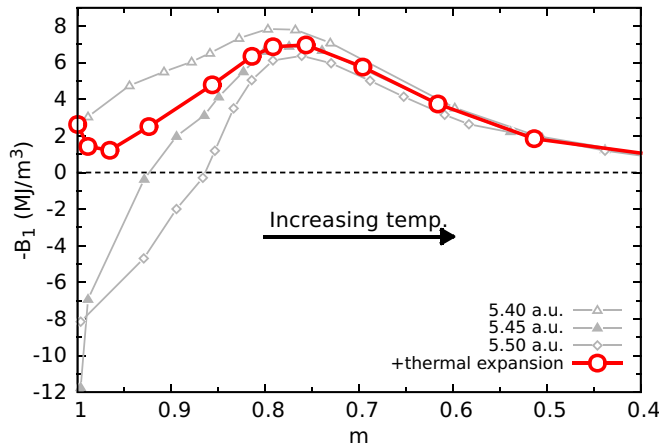
FIG. 3. The magnetoelastic constant B_1 calculated at the experimental lattice parameters taking thermal expansion into account as described in the text (red circles). The values of B_1 calculated at fixed lattice constants 5.40, 5.45, 5.50 a.u. (cf. Fig. 2) are also shown as gray symbols.

4. Consideration of thermal expansion

As noted already, the lattice parameter of bcc Fe expands from 5.40 a.u. close to 0 K to 5.47 a.u. at the Curie point [61]. Indeed, as shown in Appendix B a decrease in m from 1.0 to 0.8 corresponds to an increase in lattice constant of 0.05 a.u. which, as shown in Fig. 2, will have a major effect on B_1. We can attempt to account for this thermal expansion by interpolating the values of B_1 calculated at $a = 5.40$, 5.45, 5.50 a.u. to match the experimentally measured lattice constants (Appendix B), making sure to also account for the volume dependence of the magnetization.

Figure 3 shows the result of this interpolation. The main difference compared to the fixed-lattice calculations in Fig. 2 is an initial rapid decrease in the magnitude of B_1 as m decreases from 1.0 to 0.95. We note that this modest decrease in m corresponds to a temperature interval of 0–450 K and increase in lattice parameter of 0.02 a.u. Accordingly the interpolated value of B_1 at $m = 0.95$ lies approximately halfway between the values calculated for lattice constants of 5.40 and 5.45 a.u, -1.2 MJ m^{-3}, which is smaller than the zero-temperature value of -2.5 MJ m^{-3}. Increasing the temperature further leads to the interpolated value coinciding with the 5.45 a.u. calculation at $m = 0.8$ and then subsequently tracking the 5.45 and 5.50 a.u. calculations.

Considering again the experimental data in Fig. 2 we see that the calculations including thermal expansion effects provide an explanation for the initial decrease in B_1 at low temperature. According to the zero-temperature calculations, increasing the cubic lattice parameter pushes B_1 towards a more positive value, favoring negative magnetostriction. This sensitivity is particularly large around the experimental zero-temperature lattice parameter (Fig. 2). Therefore, as the lattice constant increases due to thermal expansion while the magnetization is effectively constant, the magnitude of B_1 decreases. At higher temperature ($m \sim 0.8$) the peak in B_1 calculated for the wide range of lattice parameters dominates. Finally, as the temperature further increases the magnetoelastic constant
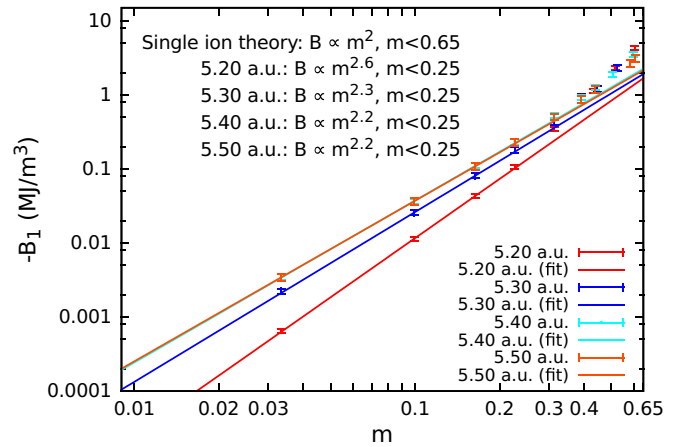

FIG. 4. The high-temperature variation in magnetoelastic constant B_1 with respect to reduced magnetization for lattice parameters between 5.20 a.u. and 5.50 a.u. for bcc Fe, plotted on a logarithmic scale and fitted to a power law Ax^γ.

reduces to zero with the magnetic order parameter, which we consider further in the next section.

At this point it is natural to ask whether experiments also observe a strong sensitivity of the magnetostriction to lattice parameter a. Experimentally, Franse *et al.* [66] determined that the application of pressure to bcc Fe increases λ_{001} at a rate of 0.8×10^{-6} kbar^{-1}. In order to calculate the rate of change of B_1 with respect to lattice parameter a we apply the chain rule to Eq. (4), deriving the expression [introducing $c' = (c_{11} - c_{12})/2$]

$$\frac{\partial B_1}{\partial a} = -3\left(\lambda_{001}\frac{\partial c'}{\partial P} + c'\frac{\partial \lambda_{001}}{\partial P}\right)\bigg/\frac{\partial a}{\partial P}. \qquad (14)$$

The pressure derivatives $\partial c'/\partial P$ [67] and $\partial a/\partial P$ [68] are 1.07 and 1.1×10^{-3} a.u. kbar^{-1}, respectively. Therefore experimentally, $\partial B_1/\partial a = -680$ MJ m^{-3} a.u.$^{-1}$. This value is indeed consistent with our calculations, which at the theoretical lattice parameter ($a = 5.20$ a.u.) give $\partial B_1/\partial a = -360$ MJ m^{-3} a.u.$^{-1}$, while at $a = 5.40$ a.u. they give $\partial B_1/\partial a = -1100$ MJ m^{-3} a.u.$^{-1}$.

5. High-temperature power-law behavior

In Fig. 4 we focus on the high-temperature behavior of the magnetoelastic constant, plotted on a logarithmic scale for lattice parameters $a = 5.20$, 5.30, 5.40, and 5.50 a.u. For $m \leqslant 0.25$ the data demonstrate good agreement with a power-law relationship, which we fit in this region as $B = Ax^\gamma$ with $\gamma = 2.2$–2.6, as shown in the figure. We recall that the high-temperature behavior expected from single-ion theory [9] is $\gamma = 2$. There is reasonable agreement between single-ion theory and the calculations, particularly at $a = 5.30$, 5.40, and 5.50 a.u., for $m \leqslant 0.25$.

It should be noted however that the m^2 behavior predicted by single-ion theory is expected to hold for $m \leqslant 0.65$, which is clearly not the case in the calculations. We also point out that both single-ion theory and the DFT-DLM picture are mean-field theories, so while there is agreement between theory and our calculations, they are unlikely to provide a
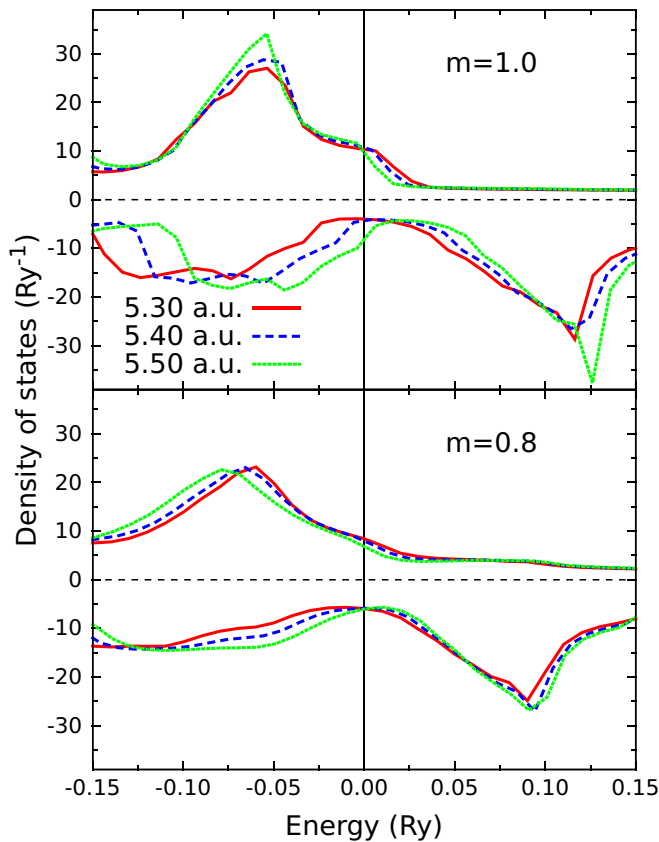
FIG. 5. The density of states for the majority and minority spin channels (positive/negative scales, respectively) in bcc Fe for $a = 5.30$ (red, solid), 5.40 (blue, dashed), and 5.50 a.u. (green, dotted), where zero energy corresponds to the Fermi energy.

full description of magnetic properties close to the Curie temperature.

6. Band-filling analysis

In order to investigate the dramatic volume dependence of B_1 at zero temperature, we plot the scalar-relativistic density of states (DOS) of bcc Fe around the Fermi energy E_f at $a = 5.30$, 5.40, and 5.50 a.u. in Fig. 5. It is clear that an increase in lattice parameter represents a positive shift of features in the minority DOS relative to E_f, while their shape remains largely unchanged (features in the majority DOS also shift, but noticeably less so). We see this in how E_f lies around the center of the large valley in the minority DOS when $a = 5.30$ a.u., whereas at 5.40 a.u. E_f is situated at the left-hand side of this valley and by $a = 5.50$ a.u. it lies outside. In terms of magnetostriction, Fig. 2 shows that λ_{001} changes sign between $a = 5.40$ and 5.50 a.u., coinciding with E_f exiting this valley. It should also be noted that while E_f lies firmly in the center of this valley, between 5.20 and 5.35 a.u., the volume dependence of B_1 is far less than it is when E_f is located around the shoulder.

To confirm the importance of the location of the Fermi level with respect to features in the electronic structure, in Fig. 6 we plot B_1 both as a function of lattice parameter (red) and band filling (blue). The latter calculations were performed by fixing $a = 5.20$ a.u. and varying the Fermi energy. There is a striking
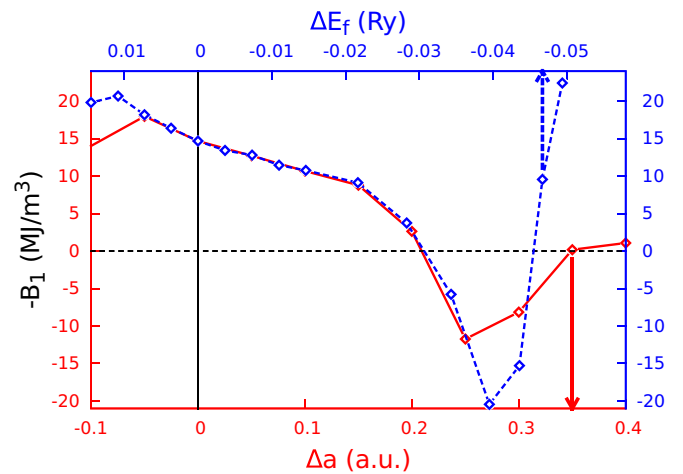

FIG. 6. The variation in zero-temperature magnetoelastic constant B_1 with respect to change in lattice parameter from $a = 5.20$ a.u. (red line and axes) and shift in Fermi energy (blue line and axes). The arrows indicate which axes the data belong to.

correlation between the two curves between 5.15 and 5.45 a.u. Outside this range, it is possible that expanding or contracting the lattice no longer represents a straightforward energy shift in the DOS and that more complex changes in the shape of the band structure become significant.

With this correlation in mind, we now turn our attention to the DOS of bcc Fe over the same range of lattice parameters at $m = 0.8$, plotted in the bottom half of Fig. 5, around which the peak in magnetostriction occurs and the volume dependence has been mostly suppressed. Here we can see that onset of some magnetic disorder has effectively washed out finer features of the DOS and introduced new ones [69]. For example, the shoulder over which E_f passes as the lattice expands when $m = 1$ is now far less well defined. This means that the environment around E_f has been somewhat homogenized with respect to different lattice parameters. This could explain the reduced volume dependence. The origin of the peak in magnetostriction is less clear however. It is possible that for $a = 5.40$ and 5.50 a.u. the local environment around E_f more resembles that seen at 5.30 a.u., where it sits inside the valley rather than at the edge, which we know corresponds to an enhancement in magnetostriction at $m = 1$.

B. *A2* $Fe_{1-x}Ga_x$

1. Zero-temperature magnetoelasticity

We now explore the effect of doping Ga into bcc Fe. We use the CPA to model the fully disordered *A2* structure, i.e., the Ga atoms are equally likely to occupy all bcc sites. Figure 7 shows the magnetoelastic constant B_1 as a function of Ga concentration, calculated at zero temperature ($m = 1$). As for pure iron (Fig. 2) we consider a range of lattice parameters, from 5.20–5.50 a.u.

The most striking feature of Fig. 7 is that the strong sensitivity of B_1 to the lattice parameter of bcc Fe ($x = 0$) is suppressed by the addition of Ga. Indeed, at $x = 0.20$ the variation in B_1 is less than 1 MJ m^{-3} between $a = 5.20$–5.50 a.u., compared to 27 MJ m^{-3} for bcc Fe. At $x = 0.20$, B_1 is ~ -5 MJ m^{-3} for all considered lattice parameters. This
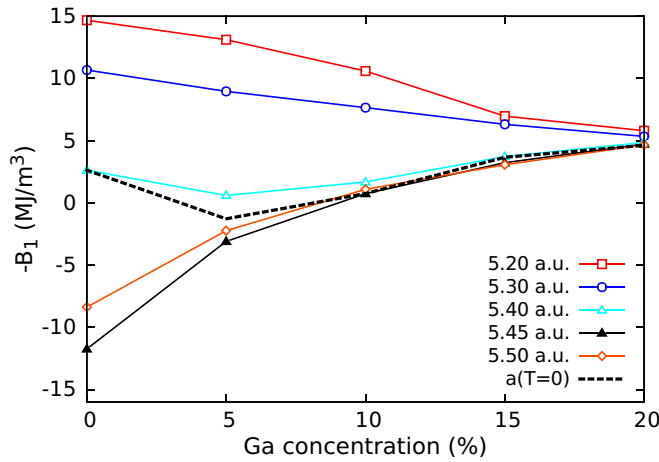
FIG. 7. The magnetoelastic constant B_1 calculated for fully disordered ($A2$) $Fe_{1-x}Ga_x$ as a function of Ga concentration, for different lattice parameters.

value represents a reduction in the magnitude of B_1 with Ga concentration for all cases except $a = 5.40$ a.u.

Similarly to what we did in Fig. 3, in order to account for the expansion of the lattice at zero temperature as a result of Ga addition we interpolate our calculations according to the experimentally measured lattice constant data in Ref. [70], which we have assumed to behave linearly between 5% and 15%. The result of this interpolation is shown as the dashed line in Fig. 7. We see that the enhancement in B_1 is less than 2 MJ m^{-3} even when taking the lattice expansion into account. Therefore, the zero-temperature calculations do not show any clear fingerprint of the $\sim 10\times$ enhancement of the magnetostriction observed experimentally [5].

2. Effect of Ga on the zero-temperature density of states

In order to investigate the suppression of the volume dependence of B_1 with Ga concentration, in Fig. 8 we plot the scalar-relativistic DOS projected onto the Fe atoms for different lattice parameters and Ga concentrations. In bcc Fe ($x = 0$), as detailed in Sec. III A 6, there are noticeable changes in the DOS close to the Fermi energy upon varying the lattice parameter due to a shift in the minority DOS features relative to E_f. The different behavior of these states when magnetized along different directions generates the MCA and magnetostriction [26]. However, increasing the Ga concentration within the CPA has the effect of smoothing over these fine features of the DOS, similarly to that seen by increasing magnetic disorder in Fig. 5. We can therefore draw close comparisons between the Ga concentration and magnetic order dependencies of B_1 over different lattice parameters. In both cases there is a decrease in volume dependence with increasing disorder (chemical and magnetic). Smaller lattice parameters (5.20–5.30 a.u.) produce a monotonic decrease in $-B_1$ with increasing disorder, while larger lattice parameters (5.40–5.50 a.u.) mostly produce an increase in $-B_1$.

3. $Fe_{1-x}Ga_x$ at finite temperature

In Fig. 9 we investigate the temperature dependence of B_1 of $A2$ $Fe_{1-x}Ga_x$ for different Ga concentrations and lattice
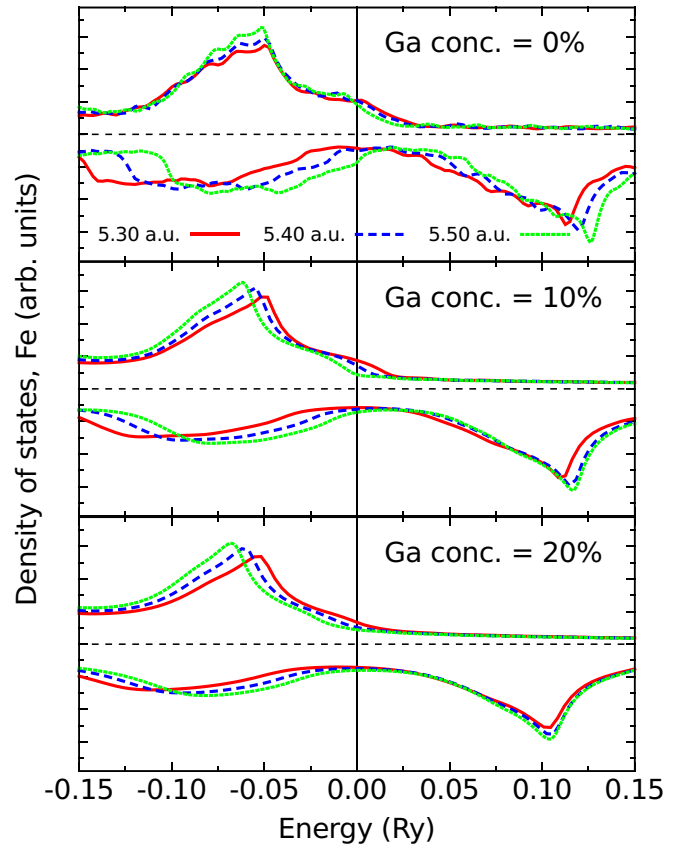

FIG. 8. The scalar-relativistic density of states projected onto the Fe atoms in $A2$ $Fe_{1-x}Ga_x$ ($x = 0, 0.1, 0.2$) for $a = 5.30$ (red, solid), 5.40 (blue, dashed), and 5.50 a.u. (green, dotted). The energy zero corresponds to the Fermi energy.

parameters. As already shown for zero temperature, increasing the Ga concentration reduces the volume sensitivity of B_1 compared to pure Fe (Fig. 2). Of particular interest is the peak in B_1 calculated to occur at $m \sim 0.7$–0.8 for pure Fe. While nonmonotonic behavior of B_1 with temperature is still observed at low Ga concentration, the peak in B_1 becomes less discernible for $x > 0.10$. Indeed, for $x = 0.20$, B_1 undergoes a monotonic decrease with temperature at all lattice constants.

Exploring the $x = 0.20$ data further, recalling that single-ion theory predicts $B(T)$ approximately $\propto m^3$ and m^2 at low and high temperatures, respectively [71], in Fig. 9 we compare the calculations against m^3 behavior (dashed line). We see that the power-law relation gives a reasonable account of the calculations. Furthermore, in the inset of Fig. 9 we replot B_1 versus temperature on a logarithmic scale. In comparison to pure Fe (Fig. 4), the high-temperature power-law dependence Ax^{γ} holds over a wider range of m ($m < 0.6$) when $a = 5.50$ a.u., with $\gamma = 2.2$ throughout.

4. Comparison with experimental data

We stress that, in light of the previous theoretical and experimental studies of Galfenol outlined in the Introduction, the neglect of short- and long-range ordering effects in the CPA calculations on the simplest $A2$ structure will unlikely provide an accurate description of its properties. In
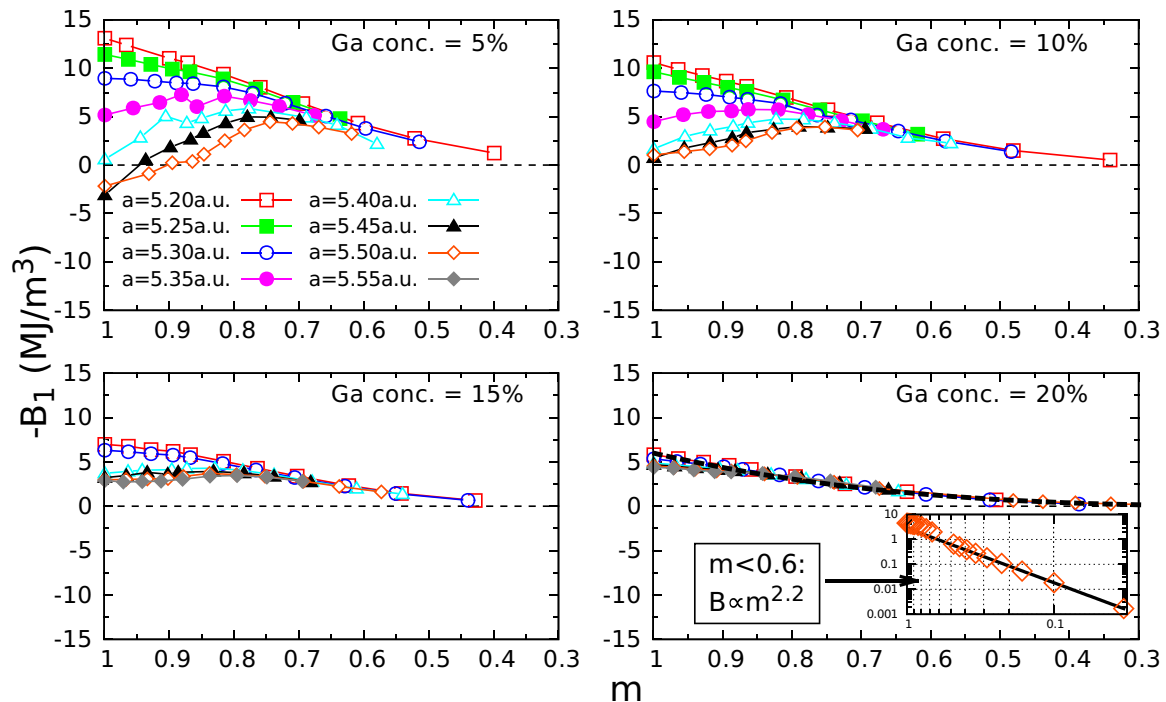
FIG. 9. The variation in B_1 with respect to reduced magnetization $m(T) = M(T)/M(0)$ for lattice parameters between 5.20 a.u. and 5.55 a.u. in $Fe_{1-x}Ga_x$ ($x = 0.05, 0.10, 0.15, 0.20$). The black, dashed curve on the $x = 0.2$ graph is a plot of $B_1(T) = B_1(T = 0)m^3$, as predicted by single-ion theory. The inset in the bottom right plot is a log-log plot of B_1 against m for $x = 0.20$ at 5.50 a.u., demonstrating the $m^{2.2}$ dependence at low temperatures.

particular, as already noted, our calculations do not show a large enhancement in the magnetoelastic constant B_1 around 19% Ga doping. Nevertheless, we still wish to make a tentative connection of our calculations to the experimental studies of the temperature-dependent magnetostriction of Galfenol reported in Ref. [72]. The authors of that work observed that the anomalous, nonmonotonic magnetoelastic temperature dependence of bcc Fe still exists at $x = 0.086$, but is no longer observed at $x = 0.166$. This result is consistent with our calculations, which show a clear suppression of the nonmonotonic thermal behavior with increasing Ga concentration. Additionally, the data in Ref. [72] show that the peak in magnetostriction exhibited at $x = 0.086$ is broader than that seen in bcc Fe, which again is reflected in our calculations. It was also observed in Ref. [72] that, at low temperatures, the temperature dependence of $Fe_{0.834}Ga_{0.166}$ is well described by the single-ion theory m^3 power law. As described in the previous section, at 20% Ga content our calculations also show good agreement with the single-ion description. These comparisons are qualitative at best and based on a limited set of data. Nevertheless, they do provide a clear motivation to study the temperature dependence of B_1 for other Fe-Ga orderings, to ascertain whether there is some universal behavior shared across the different phases.

IV. SUMMARY AND CONCLUSIONS

We have used density-functional theory in the disordered local moment picture to calculate the temperature dependence of the magnetoelastic constant B_1 for two systems: bcc Fe and fully disordered (A2) $Fe_{1-x}Ga_x$. The calculations are based on the methodology developed previously for calculating the temperature-dependent magnetocrystalline anisotropy from the magnetic torque. The current method extracts B_1 from torque calculations performed on tetragonally strained systems.

The calculations on bcc Fe revealed two key features: a strong dependence of the zero-temperature magnetostriction on the lattice constant, and a peak in the magnitude of B_1 at a magnetic ordering of $m \sim 0.7$–0.8 across a range of lattice constants. Taken together, these features provide an explanation for the experimentally observed temperature dependence of B_1: a decrease over the 0–500 K temperature range due to lattice expansion, followed by the peak at $m = 0.85$ (800 K). We note that the calculations did not find a peak in B_1 at lower temperatures, which was reported in some earlier experiments [13] but not found in more recent work [17]. The calculated sensitivity of B_1 to lattice parameter is also consistent with experimental measurements of magnetostriction under pressure [67].

The calculations on A2 $Fe_{1-x}Ga_x$ found a weakening of the magnetoelastic constant with increasing Ga content, and a suppression of the nonmonotonic temperature dependence observed for bcc Fe. The well-known enhancement in magnetostriction at 19% Ga content was absent from the calculated results, confirming that some Fe-Ga ordering seems to be necessary to provide an intrinsic explanation for the strong magnetostrictive properties of Galfenol. Nonetheless, the calculations did reproduce some experimental observations at finite temperature, specifically a simple power-law behavior in terms of $m(T)$ for a Ga content of 20%.
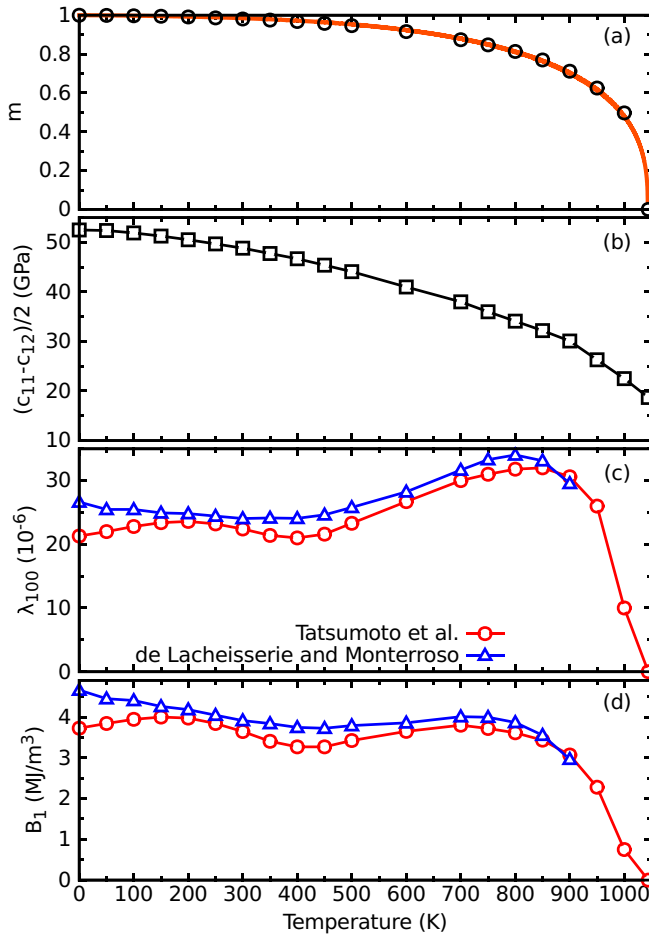
FIG. 10. Experimentally measured values of (a) reduced magnetization (Ref. [64]), (b) elastic constants (Ref. [62] for 0–300 K and Ref. [63] for > 300 K), and (c) magnetostriction λ_{001} (Ref. [13], red circles; Ref. [17], blue triangles). The line connecting the magnetization data in (a) is the function introduced in Ref. [65] as described in the text. The magnetoelastic constants calculated using Eq. (4), the elastic constants, and the two magnetostriction data sets are shown in (d).

Our calculations have shown that the peak in B_1 with temperature of bcc Fe can be explained intrinsically and correlates with electronic structure features. We have however been unable to uncover the precise electronic mechanism for its origin. What is remarkable is that at zero temperature B_1 is highly sensitive to the lattice parameter, yet this sensitivity is sufficiently suppressed by a relatively small amount of magnetic disorder ($m \sim 0.8$; cf. Fig. 2) to yield the peak in B_1 across a range of lattice constants.

The calculation method described here is sufficiently general to be applied to a range of systems, where the thermally induced magnetic excitations are adequately described in terms of fluctuating local moments and particularly where the magnetism has an itinerant origin and therefore expected to be not necessarily described by single-ion theory. Based on the current work the obvious next steps are to study ordered Fe-Ga phases, particularly in order to establish whether the addition of Ga always suppresses the nonmonotonic temperature dependence of B_1 in bcc Fe. The giant magnetostrictive
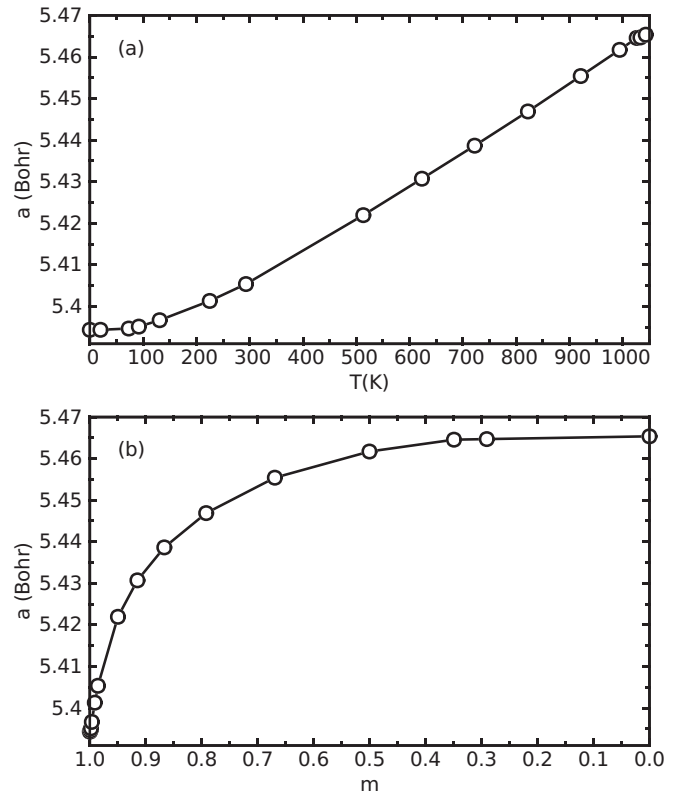

FIG. 11. Experimentally measured lattice constants of bcc Fe reported in Ref. [61] as a function of (a) temperature and (b) reduced magnetization.

Laves phase compounds $RE\text{Fe}_2$ (RE = rare earth), where the magnetism originates from both itinerant and localized electrons, also represent key test cases for the *ab initio* theory.

APPENDIX A: EXTRACTING B_1 FROM EXPERIMENT

In Fig. 10 we show the previously reported experimental data [13,17,62–65] used to derive the magnetoelastic constant B_1 of bcc Fe shown in Fig. 2 of the main text. B_1 is calculated as a function of temperature from the elastic constants and [0 0 1] magnetostriction shown in Figs. 10(b) and 10(c) using Eq. (4), and plotted in Fig. 10(d). We then use the reduced magnetization data in Fig. 10(a) to map the temperature axis onto m (Fig. 2). For this mapping it is convenient to use the parametrization of the experimental data introduced in Ref. [65], $m(\tau) = [1 - s\tau^{3/2} - (1-s)\tau^p]^{1/3}$ with $\tau = T/T_C$, $s = 0.35$, $p = 4$, and $T_C = 1044$ K. This parametrization is also shown in Fig. 10(a).

APPENDIX B: THE THERMAL EXPANSION OF BCC Fe

In Fig. 11 we show the lattice constants of bcc Fe reported in Ref. [61]. The data are reported as a function of

temperature in Ref. [61] [Fig. 11(a)]; we use the experimentally measured magnetization data and parametrization showed in Fig. 10(a) to replot the data as a function of reduced magnetization m in Fig. 11(b). This information was used in the calculations of the magnetoelastic constant accounting for thermal expansion (Fig. 3 of the main text). The factor of 1.00202×10^{-10} was used to convert kX units into meters.

[1] E. du Trémolet de Lacheisserie, *Magnetostriction: Theory and Applications of Magnetoelasticity* (CRC Press, Boca Raton, FL, 1993).

[2] R. Abbundi and A. Clark, IEEE Trans. Magn. **13**, 1519 (1977).

[3] A. Olabi and A. Grunwald, Mater. Des. **29**, 469 (2008).

[4] S. A. Wilson *et al.*, Mater. Sci. Eng.: R **56**, 1 (2007).

[5] A. E. Clark, K. B. Hathaway, M. Wun-Fogle, J. B. Restorff, T. A. Lograsso, V. M. Keppens, G. Petculescu, and R. A. Taylor, J. Appl. Phys. **93**, 8621 (2003).

[6] A. E. Clark, J. B. Restorff, M. Wun-Fogle, D. Wu, and T. A. Lograsso, J. Appl. Phys. **103**, 07B310 (2008).

[7] R. Grössinger, R. S. Turtelli, and N. Mehmood, IOP Conf. Ser.: Mater. Sci. Eng. **60**, 012002 (2014).

[8] R. J. Elliott, in *Magnetic Properties of Rare Earth Metals*, edited by R. J. Elliott (Plenum Press, London, 1972), p. 1.

[9] E. Callen and H. Callen, J. Phys. Chem. Solids **16**, 310 (1960).

[10] E. R. Callen and H. B. Callen, Phys. Rev. **129**, 578 (1963).

[11] A. E. Clark, B. F. DeSavage, and R. Bozorth, Phys. Rev. **138**, A216 (1965).

[12] E. Callen, J. Appl. Phys. **39**, 519 (1968).

[13] E. Tatsumoto and T. Okamoto, J. Phys. Soc. Jpn. **14**, 1588 (1959).

[14] H. B. Callen and E. R. Callen, Phys. Rev. **132**, 991 (1963).

[15] H. S. Belson, J. Appl. Phys. **38**, 1327 (1967).

[16] G. M. Williams and A. S. Pavlovic, J. Appl. Phys. **39**, 571 (1968).

[17] E. du Tremolet de Lacheisserie and R. M. Monterroso, J. Magn. Magn. Mater. **31–34**, 837 (1983).

[18] L. Dominguez and K. Kulakowski, J. Magn. Magn. Mater. **185**, 121 (1998).

[19] B. L. Györffy, A. J. Pindor, J. Staunton, G. M. Stocks, and H. Winter, J. Phys. F **15**, 1337 (1985).

[20] J. B. Staunton, S. Ostanin, S. S. A. Razee, B. L. Gyorffy, L. Szunyogh, B. Ginatempo, and E. Bruno, Phys. Rev. Lett. **93**, 257204 (2004).

[21] J. B. Staunton, L. Szunyogh, A. Buruzs, B. L. Gyorffy, S. Ostanin, and L. Udvardi, Phys. Rev. B **74**, 144411 (2006).

[22] M. Matsumoto, R. Banerjee, and J. B. Staunton, Phys. Rev. B **90**, 054421 (2014).

[23] C. E. Patrick, S. Kumar, G. Balakrishnan, R. S. Edwards, M. R. Lees, L. Petit, and J. B. Staunton, Phys. Rev. Lett. **120**, 097202 (2018).

[24] A. Deák, E. Simon, L. Balogh, L. Szunyogh, M. dos Santos Dias, and J. B. Staunton, Phys. Rev. B **89**, 224401 (2014).

[25] R. Wu, in *Handbook of Magnetism and Advanced Magnetic Materials*, edited by H. Kronmueller and S. Parkin (John Wiley and Sons, Ltd., Haboken, NJ, 2007).

[26] R. Wu, L. Chen, and A. Freeman, J. Magn. Magn. Mater. **170**, 103 (1997).

[27] R. Wu, L. Chen, A. Shick, and A. Freeman, J. Magn. Magn. Mater. **177–181**, 1216 (1998).

[28] R. Wu and A. Freeman, J. Magn. Magn. Mater. **200**, 498 (1999).

[29] M. Komelj and M. Fähnle, J. Magn. Magn. Mater. **220**, 8 (2000).

[30] T. Burkert, O. Eriksson, P. James, S. I. Simak, B. Johansson, and L. Nordström, Phys. Rev. B **69**, 104426 (2004).

[31] Q. Xing, T. A. Lograsso, M. P. Ruffoni, C. Azimonte, S. Pascarelli, and D. J. Miller, Appl. Phys. Lett. **97**, 072508 (2010).

[32] M. Fähnle, M. Komelj, R. Q. Wu, and G. Y. Guo, Phys. Rev. B **65**, 144436 (2002).

[33] R. Wu, J. Appl. Phys. **91**, 7358 (2002).

[34] Y. N. Zhang, J. X. Cao, and R. Q. Wu, Appl. Phys. Lett. **96**, 062508 (2010).

[35] H. Wang, Y. N. Zhang, R. Q. Wu, L. Z. Sun, D. S. Xu, and Z. D. Zhang, Sci. Rep. **3**, 3521 (2013).

[36] K. Chen and L. M. Cheng, Phys. Status Solidi B **244**, 3583 (2007).

[37] M. V. Matyunina, M. A. Zagrebin, V. V. Sokolovskiy, and V. D. Buchelnikov, J. Magn. Magn. Mater. **470**, 118 (2019).

[38] T. Khmelevska, S. Khmelevskyi, and P. Mohn, J. Appl. Phys. **103**, 073911 (2008).

[39] H. Ebert, D. Ködderitzsch, and J. Minár, Rep. Prog. Phys. **74**, 096501 (2011).

[40] A. Khachaturyan and D. Viehland, Metall. Mater. Trans. A **38**, 2308 (2007).

[41] A. Khachaturyan and D. Viehland, Metall. Mater. Trans. A **38**, 2317 (2007).

[42] H. Cao, P. M. Gehring, C. P. Devreugd, J. A. Rodriguez-Rivera, J. Li, and D. Viehland, Phys. Rev. Lett. **102**, 127201 (2009).

[43] M. Laver, C. Mudivarthi, J. R. Cullen, A. B. Flatau, W.-C. Chen, S. M. Watson, and M. Wuttig, Phys. Rev. Lett. **105**, 027202 (2010).

[44] Y. He, C. Jiang, W. Wu, B. Wang, H. Duan, H. Wang, T. Zhang, J. Wang, J. Liu, Z. Zhang, P. Stamenov, J. Coey, and H. Xu, Acta Mater. **109**, 177 (2016).

[45] Y. Du, M. Huang, S. Chang, D. L. Schlagel, T. A. Lograsso, and R. J. McQueeney, Phys. Rev. B **81**, 054432 (2010).

[46] Y. Du, M. Huang, T. A. Lograsso, and R. J. McQueeney, Phys. Rev. B **85**, 214437 (2012).

[47] C. Kittel, Rev. Mod. Phys. **21**, 541 (1949).

[48] J. B. Restorff, M. Wun-Fogle, K. B. Hathaway, A. E. Clark, T. A. Lograsso, and G. Petculescu, J. Appl. Phys. **111**, 023905 (2012).

[49] H. Zijlstra, *Experimental Methods in Magnetism* (Netherlands, Amsterdam, 1967), Vol. 2.

[50] X. Wang, R. Wu, D.-s. Wang, and A. J. Freeman, Phys. Rev. B **54**, 61 (1996).

[51] C. E. Patrick and J. B. Staunton, Phys. Rev. B **97**, 224415 (2018).

[52] See Supplemental Material at http://link.aps.org/supplemental/10.1103/PhysRevB.99.054415 for an investigation of different computational methods, specifically their impact on B_1 vs m and T_θ vs $u_z z$ curves. In addition there are data on the magnetization direction dependence of T_θ which confirms the accuracy of the linear magnetoelasticity model.

[53] J. B. Staunton, A. Marmodoro, and A. Ernst, J. Phys.: Condens. Matter **26**, 274210 (2014).

[54] E. Mendive-Tapia and J. B. Staunton, Phys. Rev. Lett. **118**, 197202 (2017).

[55] L. Petit, D. Paudyal, Y. Mudryk, K. A. Gschneidner, Jr., V. K. Pecharsky, M. Lüders, Z. Szotek, R. Banerjee, and J. B. Staunton, Phys. Rev. Lett. **115**, 207201 (2015).

[56] G. M. Stocks, W. M. Temmerman, and B. L. Gyorffy, Phys. Rev. Lett. **41**, 339 (1978).

[57] M. Däne, M. Lüders, A. Ernst, D. Ködderitzsch, W. M. Temmerman, Z. Szotek, and W. Hergert, J. Phys.: Condens. Matter **21**, 045604 (2009).

[58] S. H. Vosko, L. Wilk, and M. Nusair, Can. J. Phys. **58**, 1200 (1980).

[59] E. Bruno and B. Ginatempo, Phys. Rev. B **55**, 12946 (1997).

[60] C. E. Patrick, S. Kumar, G. Balakrishnan, R. S. Edwards, M. R. Lees, E. Mendive-Tapia, L. Petit, and J. B. Staunton, Phys. Rev. Mater. **1**, 024411 (2017).

[61] Z. S. Basinski, W. Hume-Rothery, and A. L. Sutton, Proc. R. Soc. London A **229**, 459 (1955).

[62] J. A. Rayne and B. S. Chandrasekhar, Phys. Rev. **122**, 1714 (1961).

[63] D. Dever, J. Appl. Phys. **43**, 3293 (1972).

[64] J. Crangle and G. M. Goodman, Proc. R. Soc. London A **321**, 477 (1971).

[65] M. D. Kuz'min, Phys. Rev. Lett. **94**, 107204 (2005).

[66] J. Franse, R. Winkel, R. Veen, and G. D. Vries, Physica **33**, 475 (1967).

[67] M. W. Guinan and D. N. Beshers, J. Phys. Chem. Solids **29**, 541 (1968).

[68] H. Mao, W. A. Bassett, and T. Takahashi, J. Appl. Phys. **38**, 272 (1967).

[69] J. Staunton, B. L. Györffy, A. J. Pindor, G. M. Stocks, and H. Winter, J. Phys. F **15**, 1387 (1985).

[70] N. Kawamiya, K. Adachi, and Y. Nakamura, J. Phys. Soc. Jpn. **33**, 1318 (1972).

[71] H. Callen and E. Callen, J. Phys. Chem. Solids **27**, 1271 (1966).

[72] A. E. Clark, M. Wun-Fogle, J. B. Restorff, K. W. Dennis, T. A. Lograsso, and R. W. McCallum, J. Appl. Phys. **97**, 10M316 (2005).